

# Temperature Dependent Failure of Atomically Thin MoTe<sub>2</sub>

*A S M Redwan Haider<sup>1#</sup>, Ahmad Fatehi Ali Mohammed Hezam<sup>1#</sup>, Md Akibul Islam<sup>2\*</sup>, Rafsan Al Shafatul Islam Subad<sup>3</sup>, Yeasir Arafat<sup>4</sup>, Mohammad Tanvirul Ferdaous<sup>4</sup>, Sayedus Salehin<sup>1</sup>, Md.Rezwanul Karim<sup>1\*</sup>*

<sup>1</sup>Department of Mechanical and Production Engineering, Islamic University of Technology, Bangladesh.

<sup>2</sup>Department of Mechanical and Industrial Engineering, University of Toronto, Canada.

<sup>3</sup>Department of Mechanical Engineering, University of Maryland, USA.

<sup>4</sup>Independent Researcher.

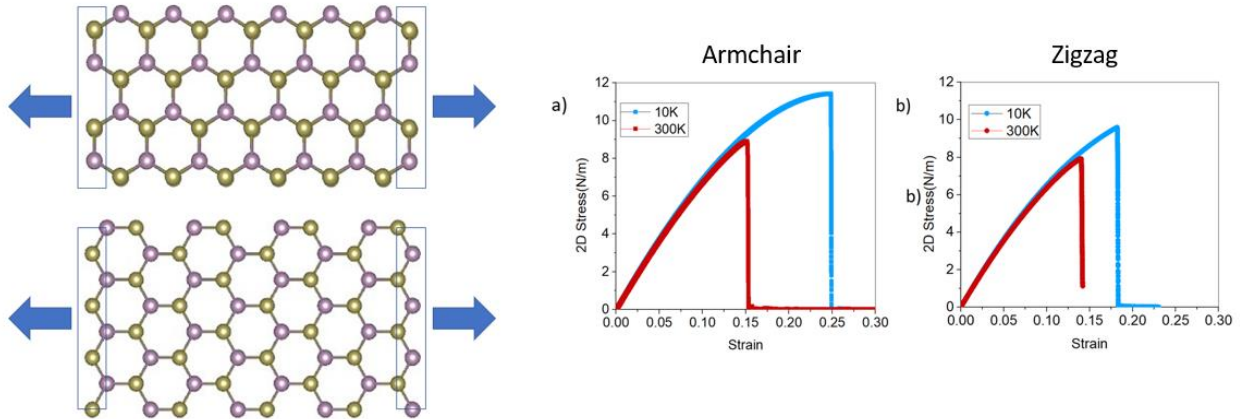
#Equal Contributions

\*Corresponding Authors

## Abstract:

In this study, we systematically investigated the mechanical responses of monolayer molybdenum ditelluride (MoTe<sub>2</sub>) using molecular dynamics simulations. The tensile behavior of trigonal prismatic phase (2H phase) MoTe<sub>2</sub> under uniaxial strain was simulated in the armchair and zigzag direction. We also investigated the crack formation and propagation in both armchair and zigzag directions at 10K and 300K to understand the fracture behavior of monolayer MoTe<sub>2</sub> at different temperatures. The crack simulations show clean cleavage for the armchair direction and the cracks were numerous and scattered in the case of the zigzag direction. Finally, we investigated the effect of temperature on Young's modulus and fracture stress of monolayer MoTe<sub>2</sub>. The results show that at a strain rate of  $10^{-4}$  ps<sup>-1</sup>, the fracture strength of 2H-MoTe<sub>2</sub> in the armchair and zigzag direction at 10K is 16.33 GPa (11.43 N/m) and 13.71429 GPa (9.46 N/m) under a 24% and 18% fracture strain, respectively. The fracture strength of 2H-MoTe<sub>2</sub> in the armchair and zigzag direction at 600K is 10.81 GPa (7.56 N/m) and 10.13 GPa (7.09 N/m) under a 12.5% and 12.47% fracture strain, respectively.

## Graphical Abstract:



**Keywords:** 2D materials, Molybdenum ditelluride, molecular dynamics, Stillinger Weber potential, Fracture mechanics.

---

## 1. Introduction

Since the discovery of graphene in 2004[1], atomically thin two-dimensional materials have garnered great interest due to their excellent mechanical[2], electrical[3], thermal [4], optical [5] anti-corrosive [6] and magnetic properties[7]. While graphene has been confirmed as the strongest material ever measured, its inherent lack of a band gap has constrained its utility in the semiconductor industry, thus it is difficult to use in transistor applications [1] and bioelectronics [8]. Transition metal dichalcogenides (TMDCs) hence emerged as a promising candidate for transistor applications due to the presence of direct and indirect band gap in their atomic structure[9]–[11]. A TMDC is a sandwich structure where a metal atom (M) is sandwiched between two chalcogen atoms (X) in hexagonal layers and is represented as  $\text{MX}_2$ . Group VI TMDCs (Mo and W) are of particular interest due to more than one possible 2D crystal structure. These materials have become a key component in the flexible and wearable electronics industry [12], [13]. TMDCs have specific mechanical and structural properties that enables researchers to develop lateral heterostructures which gives rise to flexibility in the development of electronic devices [14]–[16]. The preliminary studies conducted on mechanical characteristics of TMDCs were focused on obtaining properties such as young's modulus of pristine  $\text{MoS}_2$  obtained using exfoliation techniques [17]–[19]. One of these structural phases is semiconducting and the other one is metallic [20]–[22]. This is an interesting property since the semiconducting phase can be used to make electronic devices[20] and the metallic phase can be used in catalytic activities leading to hydrogen evolution[23]–[25]. It has been suggested in the literature that the phase transition between the semiconducting and metallic phases is possible using controlled strain[26]. Among all the TMDCs,  $\text{MoS}_2$  has received the most attention in this aspect. However,  $\text{MoS}_2$  may not be the best candidate for strain-induced phase transition due to the high energy required for the transition ( $\Delta E > 0.8 \text{ eV}$ )[26]. In contrast,  $\text{MoTe}_2$  exhibits a significantly smaller energy difference between its semiconducting and metallic phase ( $\Delta E < 50 \text{ meV}$ ) [26], [27]. Hence, it is of utmost importance to investigate the mechanical properties of monolayer  $\text{MoTe}_2$  under controlled strain to determine the stability and durability of this TMDC. Based on optical absorption spectra at a temperature of 4.2 Kelvin, it has been determined that 2H- $\text{MoTe}_2$  possesses an indirect band gap of approximately  $1.06 \pm 0.01 \text{ eV}$ . In contrast, 1T'- $\text{MoTe}_2$  displays semi-metallic behavior under the same conditions [28].  $\text{MoTe}_2$  has recently been used in a wide range of applications ranging from photodetectors [29], and energy storage [30] to novel piezoelectricity

[31]. Claudia et al [32] have characterized the single layer and multilayer MoTe<sub>2</sub> by using photoluminescence, optical absorbance and Raman scattering. The results suggest that the monolayer of MoTe<sub>2</sub> has an optical band gap of 1.10 eV which is quite high in comparison to bulk or multilayered MoTe<sub>2</sub>. The advancement of photodetectors and solar cells is fascinating findings, such as the achievement of higher power efficiency to up to 8.94% due to the addition of 10 vol% proportion of MoTe<sub>2</sub> nanostructures in PBDB-T:ITIC polymer matrix as an active layer [28]. TMDs have been incorporated in field-effect resistors since 2004, as they exhibited ambipolar behavior with high mobility and current modulation. Conan et al [33] deduced that the mobility of the bulk MoTe<sub>2</sub> can reach up to 200 cm<sup>2</sup> V<sup>-1</sup> s<sup>-1</sup> at room temperature. Controlled growth conditions were used to synthesize materials on MoTe<sub>2</sub> crystals for the development of light-emitting transistors [34]. Another fascinating property of monolayer MoTe<sub>2</sub> is its flexibility and stretchability, making it possible to apply external deformation to manipulate their physical properties [29]. The flexibility allows device to be subjected to bending and stretching and thus can be used to manufacture bendable screens, electronic paper, electronic skin and wearable biosensors [35], [36]. Among all the TMDCs, molybdenum ditelluride (MoTe<sub>2</sub>) has attracted special attention due to the possibility of phase transition between two stable phases- semiconducting 2H (hexagonal; ~1 eV bandgap) and metallic 1T (octahedral)[27], [37]–[39]. The first principal energy calculations revealed that MoTe<sub>2</sub> has a smaller energy difference between 2H and 1T phases than other TMDCs. The literature has reported that monolayer 2H-MoTe<sub>2</sub> can be phase transitioned to 1T- MoTe<sub>2</sub> using only 3% strain [26]. This paves the way for the low energy transition between semiconducting and metallic phase which can be useful in-memory applications [40],[41]. Atomic force microscopy (AFM) has been recently used to demonstrate the phase transition in MoTe<sub>2</sub> using the nanoindentation method[41]. However, due to the instability of MoTe<sub>2</sub> in ambient air [42], it is difficult to conduct a detailed study on the phase transition and the mechanics of monolayer MoTe<sub>2</sub>. Molecular dynamics offers a unique opportunity to perform experiments on the 2D MoTe<sub>2</sub> in an environment that prevents it from exposing to air. Multiple simulations can be conducted on the same material to predict the outcome before performing hands-on experiments. However, it is worth mentioning that atomic force microscopy (AFM) based nanoindentation techniques have been used to measure the elastic properties of a few layers of MoTe<sub>2</sub> [43] and not the monolayers which are of most interest. The mechanical response of 2H, 1T, and 1T'-MoTe<sub>2</sub> to uniaxial tensile conditions were investigated

using DFT [44]. Initially, these 2D layers demonstrated a linear response, which was followed by a non-linear trend up to the ultimate tensile stress. Understanding the fracture mechanics of TMDs such as MoTe<sub>2</sub> is essential for design and engineering of nano-devices [45]–[48]. The fracture patterns due to different stress conditions help to predict the reliability and durability of such devices. Predicting the failure modes will help researchers to prevent catastrophic failures by identifying the weak points develop preventive measures [49]. The purpose of this work is to discuss the deformation and fracture behavior of monolayer 2H-MoTe<sub>2</sub> at a wide range of temperatures. The stress-strain response of 2D materials is unique compared to their bulk counterpart [49]. To mimic the mechanical properties of MoTe<sub>2</sub> using the parameterized SW interatomic potential developed by Prof Jiang [50]. Then we applied uniaxial strain [51] using molecular dynamic (MD) simulation along the zigzag and armchair direction until the monolayer fails. Analysis of stress-strain responses beyond the linear elastic regime reveals directional anisotropy in mechanical behavior and failure qualities. Finally, we varied the temperature from 100K to 600K to investigate the elastic and failure properties in monolayer 2H-MoTe<sub>2</sub>. Although experimental results on MoTe<sub>2</sub> are limited for a wide range of temperatures, we have found that young's modulus agrees with results with existing literature for pristine MoTe<sub>2</sub> [50], [52]. For 2H-MoTe<sub>2</sub> in both armchair and zigzag directions, the fracture stresses, fracture strengths and Young's modulus fall as the temperature rises, resulting from the increased atomic thermal vibrations.

One of the stable phases of monolayer MoTe<sub>2</sub> is the 2H phase, as shown in Figure 1. Here hexagonally arranged, each molybdenum atom is sandwiched between two layers of tellurium atoms forming a Te-Mo-Te sequence. Each Mo atom has six Te atoms as its first neighbors, and each Te atom is directly bound to three Mo atoms in the trigonal prismatic coordination of the intralayer atoms (Mo and Te atoms within a single layer) as shown in figure 1. Te and Mo are bonded by strong covalent bonds. The covalent bonds are predominantly governed by three bond-stretching (Mo–Te, Mo–Mo, and Te–Te) and three angle-bending motions (two Mo–Te–Te angles with Mo being the central atom and one Te–Mo–Mo). For the convenience of creating the structures in MD, we used a hexagonal unit cell ( $a=b=3.159 \text{ \AA}$  and  $c=13.964 \text{ \AA}$   $\alpha =\beta=90^\circ$  and  $\gamma=120^\circ$  [53]).

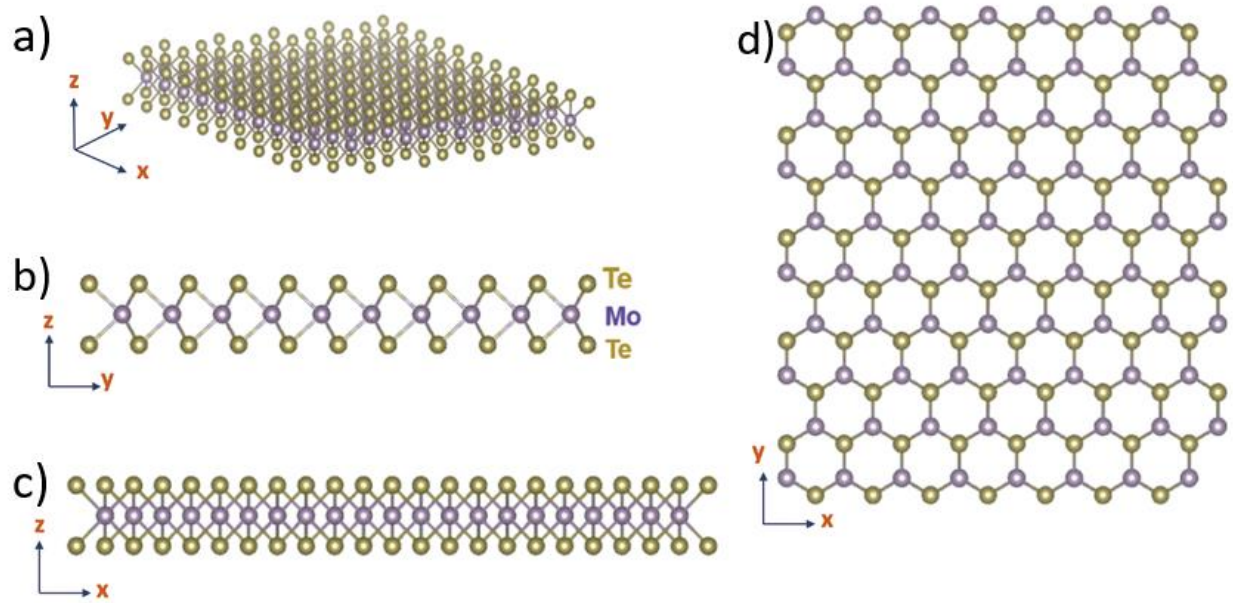


Figure 1: The crystal structure of monolayer MoTe<sub>2</sub> showing a layer of molybdenum atoms (purple) sandwiched between two layers of Tellurium atoms (olive). a) Orthogonal View, b) Front View, c) Side View and d) Top View.

## 2. Computational Method

In this section, we introduce the simulator software that was used to perform the simulations along with the essential working conditions and environment that were required to run the simulation. The description of the MoTe<sub>2</sub> structure that was used is also provided describing the bond lengths, angles and total dimensions of the sheet. Additionally, the governing equations of the model are provided.

### 2.1 Modelling monolayer 2H-MoTe<sub>2</sub>

*LAMMPS (Large-scale Atomic/Molecular Massively Parallel Simulator)* is used to carry out MD simulations [54]. It can model Nano-scale to macroscopic systems using various atomic potentials and boundary conditions. In our work, Stillinger–Weber (SW) potential is used [50], which describes the interaction of atoms inside a TMD and the coupling between them. SW potential parameters are parameterized for different materials [45] to develop a better interatomic potential, for describing the structural, mechanical and phonon spectrum of several materials [48],[55]. There

are two inequivalent bond angles in any hexagonal molybdenum dichalcogenides unit cell. Since the values are very close, a single bond angle is considered for simplification of the calculation. The modification done in the literature gives a reasonably accurate result for MoS<sub>2</sub> [55]. After the modification, Jiang et al [55] tested the strain-induced buckling on a composite TMD heterostructure. The parameterized SW potential was also used to perform simulation on materials such as monolayer Indium Selenide (InSe) [56], Tungsten Di selenide (WSe<sub>2</sub>) [57] and Borophene [58].

Figure 1 shows that the MoTe<sub>2</sub> structure has a Molybdenum (Mo) connected to a trigonal prism of six tellurium. The bond length of Mo-Te is approximately taken as 2.73 Å. Each Tellurium (Te) is surrounded by ten other Te atoms. Six Te atoms have a bond length of 3.52 Å in plane (001), one directly below is at 3.63 Å and three above it is at 3.92 Å [53]. The bond angles of Te-Mo-Te are 83.5°, 80.4° and 133.9° [53]. However, due to the parameterization of SW potential the two inequivalent bond angles are taken as equal 80.581° [59]. In the simulation a 30 nm \* 30 nm MoTe<sub>2</sub> sheet is used which was prepared using VESTA [60] that contains 25800 atoms in total [50]. The thickness of monolayer of MoTe<sub>2</sub> is considered to be 0.7 nm [61]. Periodic boundary conditions are applied in all directions, and a vacuum thickness of 30 Å is used to prevent interactions of atoms at opposite edges.

In our computational study, we utilized LAMMPS (Large-scale Atomic/Molecular Massively Parallel Simulator) to conduct molecular dynamics simulations on a 2H-MoTe<sub>2</sub> monolayer sheet. We defined several variables essential to the simulation, such as temperature, which we varied from 10 K to 600 K. Other parameters such as pressure (1 Bar), timestep (set to 0.001 fs), strain rate (10<sup>-4</sup> ps<sup>-1</sup>) were kept constant for each simulation of each separate temperature [62], [63].

In our approach, we employed a two-stage optimization process. First, we performed a geometry optimization at absolute zero using the conjugate gradient method. We then thermally equilibrated the system in an NPT ensemble for various time durations as required for a stable material. After relaxation, we applied a uniform uniaxial tensile force to the MoTe<sub>2</sub>, inducing a uniform displacement across the structure. During the MD simulation, we utilized an NPT ensemble, maintaining the number of atoms, system pressure, and temperature constant, while the volume was allowed to fluctuate. The damping constants for both the temperature and pressure are 20

picoseconds. The relaxation of the structure for temperature, potential energy, and total energy with each step refers to how these properties evolve over time as the system reaches a state of equilibrium. The strain is applied in the y-direction while the box boundaries are allowed to fluctuate in the x-direction, preserving the desired temperature and pressure. During this phase, the system's response to the applied strain, such as changes in the pressure tensor and the strain value itself, are continuously monitored and recorded.

## 2.2 Stress-strain relation and distribution

The stress-strain curves are obtained by deforming the simulation box uniaxial and calculating the average stress over the structure. Atomic stress was calculated based on the definition of virial stress. Virial stress components are calculated using [64], [65]:

$$\sigma_{\text{Virial}}(r) = \frac{1}{\Omega} \sum_i [(-m_i \dot{u}_i \otimes \dot{u}_i + \frac{1}{2} \sum_{j \neq i} r_{ij} \otimes f_{ij})] \quad (1)$$

The summation is upon all the atoms in the total volume  $\Omega$ ,  $m_i$  is the atomic mass  $i$ ,  $\dot{u}_i$  is the time derivative which indicates the displacement of atom concerning a reference position,  $r_{ij}$  is the position vector of atom,  $\otimes$  is the cross product, and  $f_{ij}$  is the interatomic force applied on atom  $i$  by atom  $j$ . Here, the Stillinger-Weber (SW), potential was used to define the interatomic interactions[50]. The SW potential comprises two-body and three-body terms describing bond stretching and breaking.

The mathematical expressions used to calculate the components of the virial stress:

$$\phi = \sum_{i < j} V_2 + \sum_{i > j < k} V_3 \quad (2)$$

$$V_2 = A e^{\left[ \frac{\rho}{r - r_{\text{max}}} \right]} \left( \frac{B}{r^4} - 1 \right) \quad (3)$$

$$V_3 = K \epsilon e^{\frac{\rho_1}{r_{ij} - r_{\text{max}ij}} - \frac{\rho_2}{r_{ik} - r_{\text{max}ik}}} (\cos \cos \theta - \cos \cos \theta_0)^2 \quad (4)$$

Here  $V_2$ , and  $V_3$  are the two-body bond stretching and angle bending terms accordingly. The terms  $r_{max}$ ,  $r_{maxij}$ ,  $r_{maxik}$  are cut-off ratios and  $\theta_0$  at the equilibrium configuration is the in-between angle of the two bonds. A and K are energy-related parameters based on the Valence Force Field (VFF) model.  $B, \rho, \rho_1$  and  $\rho_2$  are other parameters that are fitted coefficients. A and K are two energy parameters. Such parameters along with the corresponding values, were extracted from Li et al [50], [66] .

The stress can be calculated using:

$$\sigma = \frac{P_{xx} * L_y * L_z}{L_{y0} * L_{z0}} \quad (5)$$

$P_{xx}$  is the Tensile load

The strain can be calculated using:

$$\varepsilon = \frac{L_x - L_{x0}}{L_{x0}} \quad (6)$$

$L_x$  is the instantenous length of MoTe2 along  $x - axis$ .

$L_{x0}$  is the undeformed length of MoTe2 along  $x - axis$ .

The stress produced was divided by this number to calculate the plane stress using:

$$Plane\ Stress = \frac{Stress}{thickness} \quad (7)$$

### 3. Results

In order to investigate the fracture process in the 2H-MoTe<sub>2</sub>, we subjected the sheet under uniaxial tension as shown in figure 7 and increased the strain until the sheet completely fractured. We used 10K and 300K temperature initially to understand the effect of temperature on the fracture behavior of the 2D sheet. At 10K, we strained the 2D MoTe<sub>2</sub> along the armchair and zigzag edges from 0% to 24.83% and the stress in the 2D MoTe<sub>2</sub> increased from 0 to ~12 GPa. Although the entire sample surface is subjected to uniform tension deformation, thermal variations at the limited temperature cause the atomic stresses not to be distributed uniformly. Using the visualizations created by OVITO [67], it's clear that the crack propagation varies significantly between armchair and zigzag directional loading.

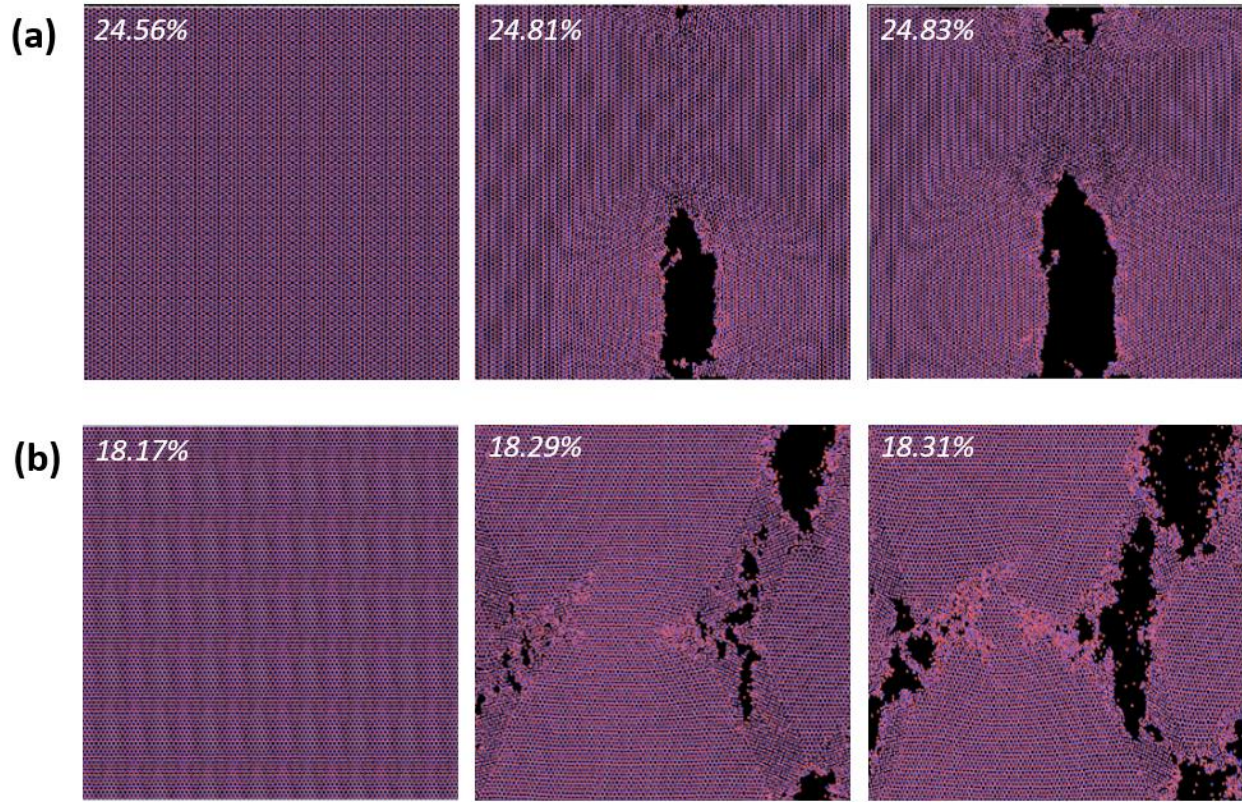


Figure 2: Crack nucleation and propagation in 2D MoTe<sub>2</sub> along the (a) armchair and (b) zigzag edges at 10K.

It is observed in Figure 2(a) that along the armchair direction, a small crack starts to nucleate at 24.81% strain by breaking of atomic bonds. The crack starts to propagate as the strain is increased without showing any sign of plasticity in the 2D sheet. Most pristine 2D materials tend to exhibit brittle failure when subjected to additional strain [68]. Here, we observe a crack, but this crack doesn't propagate through the material therefore the material does not fail completely. The sheet does not fail completely, even at 24.83% strain. A similar characteristic is observed along the zigzag edges at 10K temperature Figure 2(b). We increased the strain from 0% to 18.31% and the stress in the 2D sheet increased from 0 to ~10 GPa. A small crack starts to nucleate at 18.17% strain which starts a brittle failure, and the sheet completely fails at 18.31% strain. It is to be noted that, unlike the armchair edge, the fracture along the zigzag edge was not a clean cleavage. This shows that the fracture preferentially along a puckered groove for loads in the armchair direction rather than across the grooves. Zigzag edge images suggested that the material tend to fracture

diagonally across the sheet of material due to the distribution of forces components in two directions. Similar fracture pattern was observed in the case of uniaxial stretching of single-layer MoS<sub>2</sub> [69]. Additionally, the fracture occurred at a lower strain along the zigzag edge than the armchair edge. There is a significant difference in the fracture strain of armchair edge and zigzag edge of MoTe<sub>2</sub> at 10K, however the fracture strain values are closer in case of 300K temperature.

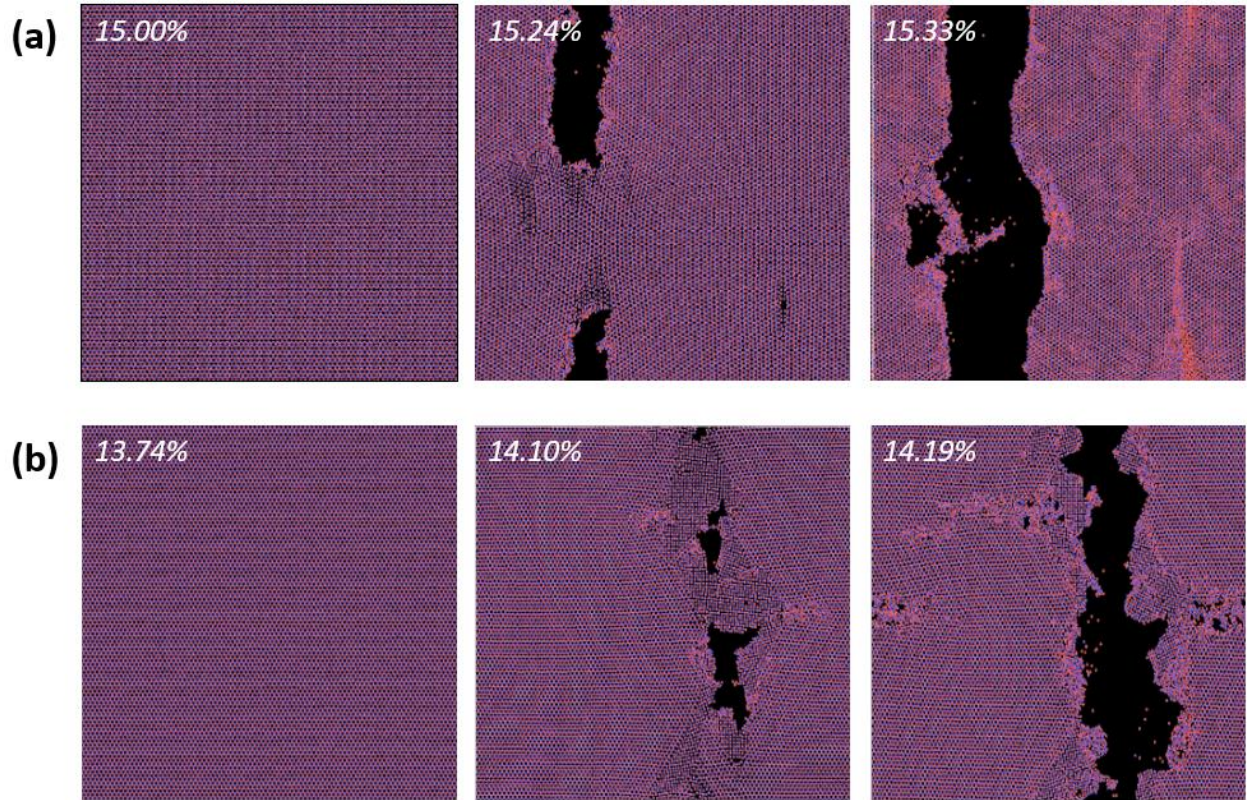


Figure 3: Crack nucleation and propagation in 2D MoTe<sub>2</sub> along the (a) armchair and (b) zigzag edges at 300K

Afterwards, we increased the temperature to 300K and applied a similar uniaxial strain on the 2D MoTe<sub>2</sub> sheet along the armchair and zigzag edge as shown in Figure 3. For the armchair direction, the crack started to nucleate at 15.2% strain and then cleaved suddenly into two clean pieces at 15.33% strain (Figure 3a). This is indicative of the same brittle behavior as before at elevated temperatures. The fracture 2D stress recorded was  $\sim 8.5$  N/m. However, in the zigzag direction, the crack started to nucleate at 14.1% strain and failed at 14.19%. The fracture 2D stress was recorded at  $\sim 8$  N/m (Figure 3b). In both figures 2 and 3 rippling were observed due to the bucking of outer Te layers. Since the poisson's ratio is positive, when the 2D sheet is stretched in one-side it produces

a compression on the other direction [70] . Therefore, the compression leads to a bucking effect. The stress-strain relations of both edges are shown in Figure 4. The results of simulation are in coherence with Prof Jiang’s stress-strain analysis of MoTe<sub>2</sub> [50].

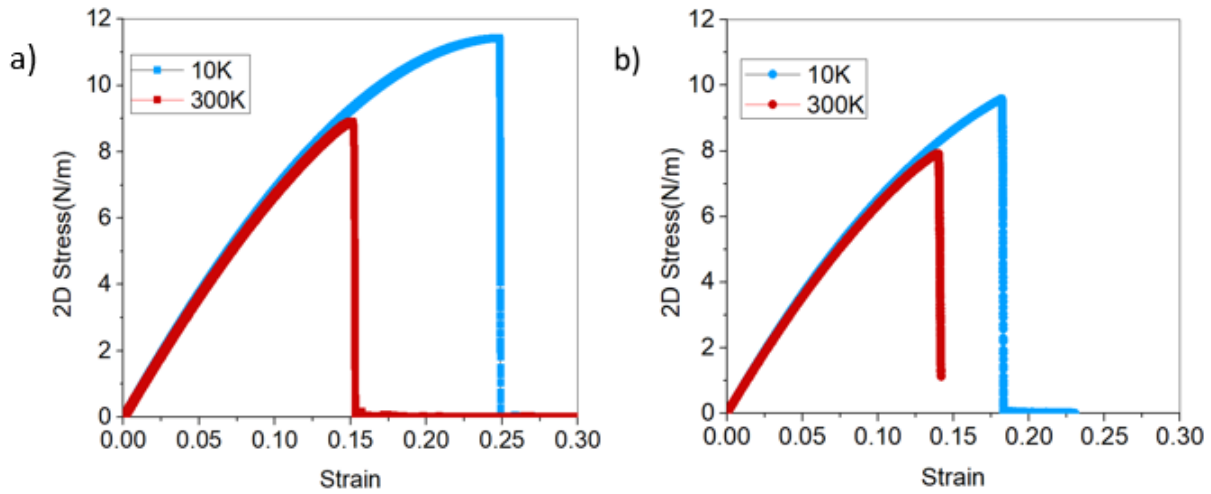


Figure 4: Stress-strain curve of a monolayer MoTe<sub>2</sub> under uniaxial tension along (a) armchair and (b) zigzag directions at 10K and 300K.

Next, we investigate the effect of varying temperatures on the physical properties of 2D MoTe<sub>2</sub> under uniaxial tension. In addition to our simulations at temperatures 10K and 300K, we also simulated the fracture behavior for 100K to 600K temperatures. The temperature showed a significant impact on the physical properties of 2D sheets. The results suggest that the fracture properties of MoTe<sub>2</sub> are sensitive to temperature. The stress-strain relationships are illustrated in Figure 5.

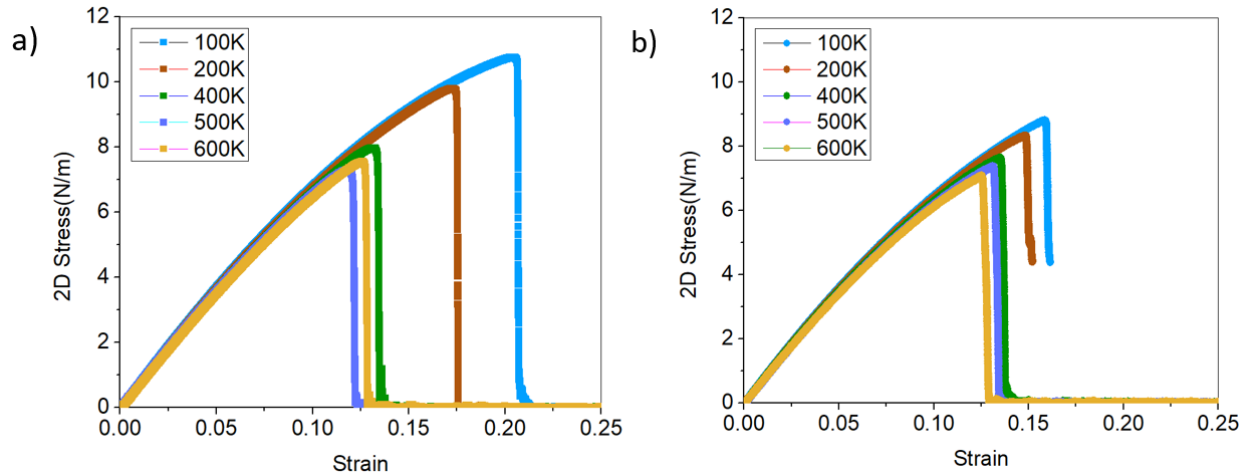


Figure 5: Stress-strain curve of a monolayer MoTe<sub>2</sub> under uniaxial tension along (a) armchair and (b) zigzag directions at different temperatures.

Note that even at elevated temperatures, the 2D sheet undergoes a brittle fracture without showing any sign of plastic deformation. Figure 5 also shows that the ultimate strain falls with increasing temperature due to the presence of high thermal vibrations [71]. The fracture strength of MoTe<sub>2</sub> was reduced by ~34% and ~26% in the armchair and zigzag direction, respectively with the increase of temperature. The fracture strain was reduced by ~49.5% and ~31% in the armchair and zigzag directions, respectively. The fracture strength and Young's Modulus is significantly lower in the case of zigzag direction in comparison to armchair direction. The relation between the 3D young's modulus, 3D fracture strength, fracture strain, and temperature are shown in Figure 6 (a-c).

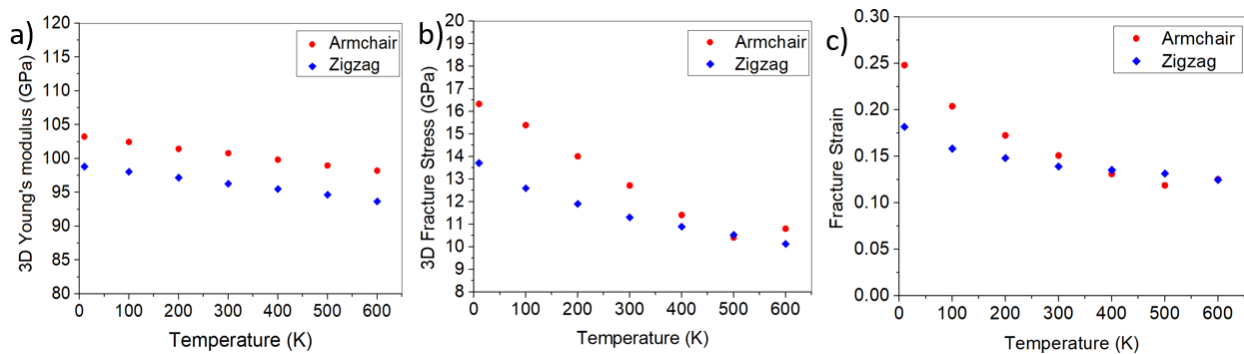


Figure 6: (a) Elastic modulus, (b) Fracture strength, and (c) Fracture strain of monolayer MoTe<sub>2</sub> at different temperatures.

We observed a difference in fracture mechanism of MoTe<sub>2</sub> due to the armchair and zigzag loading conditions. With the aid of OVITO visualizer, it can be seen that the armchair and zigzag loading have a perceptible difference in crack initiation and propagation as uniaxial tensile stress is applied.

The images in figure 7 portray the loading conditions with the bonds that are affected during the cracking period. The results suggest that the crack initiates at a higher strain in case of armchair loading in comparison to the zigzag loading. We have analyzed the bonds and the angles between Mo-Te from a planar view.

The bond breaks in the armchair loading are at 0° with the direction of loading therefore the crack occurs from the middle of the sheet. However, the zigzag loading is at 30° with the direction of loading therefore the applied stress becomes a part of the actual stress in the direction of loading. Hence, there is a diagonal fracture pattern in the sheet of the material.

In order to provide a comprehensive understanding of the research finding, we compared our obtained results with previously reported mechanical properties of monolayer transition-metal-dichalcogenides (TMDs). In Table 1 we reported the Young's Modulus and Fracture Strength of various TMDs with armchair edge at temperature of 300K. The data recorded was obtained from MD simulations and experimental techniques. These results contribute to comprehensive understanding of mechanical properties of such materials, enhancing the insight into their potential applications.

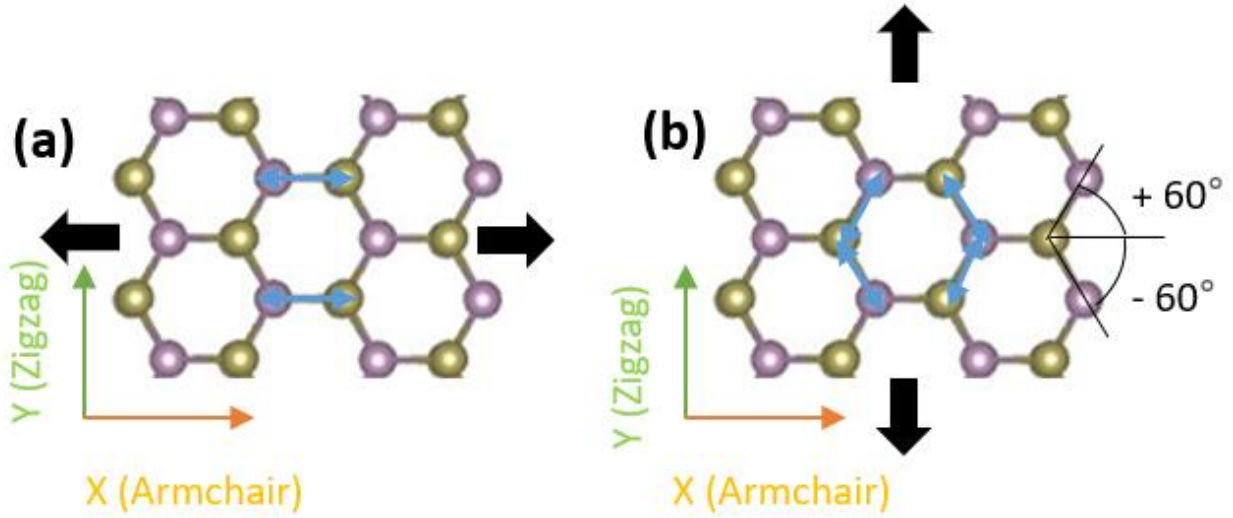


Figure 7: Planar view of the bonds in the structure that are affected most by the applied stress of 1H- MoTe<sub>2</sub> when the loading is in (a) armchair direction (b) zigzag direction. The Blue arrows show the affected bonds during propagation.

Table 1: The Young's Modulus and Fracture Strength of TMDs for armchair edge at 300K temperature using experimental and MD simulations.

2D Materials	Young's Modulus, Y (TPa)	Fracture Strength, $\sigma_{max}$ (GPa)	Approach
MoS <sub>2</sub>	0.158	12.5	MD Simulation [72]
	0.155	11.5	MD Simulation [73]
	0.159	15.03	MD Simulation [69]
	0.135	12.00	MD Simulation [52]
	0.264	-	Experimental [74]
	0.116	14.74	MD Simulation [75]
WS <sub>2</sub>	0.107	19.16	MD Simulation [76]
	0.182	19.46	MD Simulation [77]
	0.272	-	Experimental [74]

WSe <sub>2</sub>	0.119	16.20	MD Simulation [63]
	0.126	15.95	MD Simulation [78]
	0.167	-	Experimental [79]
MoSe <sub>2</sub>	0.177	2.9	Experimental [80]
	0.154	17	MD Simulation [52]
	0.100	12.95	MD Simulation [75]
MoTe <sub>2</sub>	0.121	18	MD Simulation [52]
	-	14.5	MD Simulation [38]
	0.102	12.85	This Work

#### 4. Conclusion

The fracture behaviors of a monolayer of molybdenum ditelluride (2H-MoTe<sub>2</sub>) have been investigated using molecular dynamics simulations. The fracture test was simulated under varying temperatures for both armchair and zigzag directions. Our conclusions are:

- (a) Temperature plays a significant role of the fracture mechanics of MoTe<sub>2</sub>. The stress-strain plot depicts that their property diminished with increasing temperatures. This is an important consideration when applying these 2D materials for high temperature applications.
- (b) The visual results of simulation reveal the difference in crack formation patterns for armchair and zigzag directions. Uniaxial stress in armchair directions projects a clean and fine crack on the sheet. Whereas, the same stress applied to zigzag direction initiated multiple distorted cracks.
- (c) It is found that the Young's Modulus, fracture strength and fracture strain are strongly anisotropic.

**Author contributions:** ASM R. H and A. F. A. H modeled the experiments in the simulator and conducted the experiments. ASM R. H and A.F.A. H wrote the manuscript. M.T.F and R.A.S helped to run the simulations. M.R.K, S.S, M.T.F and M.A.I helped to review the manuscript. M.R.K, S.S, Y.A, M.T.F and M.A.I supervised the work. All authors discussed the results and reviewed the final manuscript.

**Competing interests:** The authors declare that they have no competing interests. Data and materials availability: All data needed to evaluate the conclusions in the paper are present in the paper. Additional data related to this paper may be requested from the authors.

**Acknowledgement:** The authors would like to acknowledge Prof. Jin-Wu Jiang from Shanghai Institute of Applied Mathematics and Mechanics, Shanghai University and Dr. Arash from Bilkent University, Turkey for their valuable guidance and support.

## Bibliography:

- [1] K. S. Novoselov *et al.*, "Two-dimensional gas of massless Dirac fermions in graphene," *Nature*, vol. 438, no. 7065, pp. 197–200, Nov. 2005, doi: 10.1038/nature04233.
- [2] C. Lee, X. Wei, J. W. Kysar, and J. Hone, "Measurement of the elastic properties and intrinsic strength of monolayer graphene," *Science (1979)*, vol. 321, no. 5887, pp. 385–388, Jul. 2008, doi: 10.1126/SCIENCE.1157996/SUPPL\_FILE/LEE-SOM.PDF.
- [3] B. Uchoa and A. H. Castro Neto, "Superconducting states of pure and doped graphene," *Phys Rev Lett*, vol. 98, no. 14, 2007, doi: 10.1103/PhysRevLett.98.146801.
- [4] A. A. Balandin *et al.*, "Superior thermal conductivity of single-layer graphene," *Nano Lett*, vol. 8, no. 3, pp. 902–907, Mar. 2008, doi: 10.1021/NL0731872/ASSET/IMAGES/MEDIUM/NL-2007-031872\_0005.GIF.
- [5] L. A. Falkovsky and L. D. Landau, "Optical properties of graphene," *J Phys Conf Ser*, vol. 129, no. 1, p. 012004, Oct. 2008, doi: 10.1088/1742-6596/129/1/012004.
- [6] T. Qureshi *et al.*, "Graphene-based anti-corrosive coating on steel for reinforced concrete infrastructure applications: Challenges and potential," *Construction and Building Materials*, vol. 351. Elsevier Ltd, Oct. 10, 2022. doi: 10.1016/j.conbuildmat.2022.128947.
- [7] A. Varykhalov *et al.*, "Electronic and magnetic properties of quasifreestanding graphene on Ni," *Phys Rev Lett*, vol. 101, no. 15, p. 157601, Oct. 2008, doi: 10.1103/PHYSREVLETT.101.157601/FIGURES/4/MEDIUM.
- [8] C. Deepa, L. Rajeshkumar, and M. Ramesh, "Preparation, synthesis, properties and characterization of graphene-based 2D nano-materials for biosensors and bioelectronics," *Journal of Materials Research and Technology*, vol. 19, pp. 2657–2694, Jul. 2022, doi: 10.1016/J.JMRT.2022.06.023.
- [9] X. Su *et al.*, "Bandgap engineering of MoS<sub>2</sub>/MX<sub>2</sub> (MX<sub>2</sub> = WS<sub>2</sub>, MoSe<sub>2</sub> and WSe<sub>2</sub>) heterobilayers subjected to biaxial strain and normal compressive strain," *RSC Adv*, vol. 6, no. 22, pp. 18319–18325, Feb. 2016, doi: 10.1039/C5RA27871F.
- [10] H. J. Conley, B. Wang, J. I. Ziegler, R. F. Haglund, S. T. Pantelides, and K. I. Bolotin, "Bandgap engineering of strained monolayer and bilayer MoS<sub>2</sub>," *Nano Lett*, vol. 13, no. 8, pp. 3626–3630, Aug. 2013, doi: 10.1021/NL4014748/SUPPL\_FILE/NL4014748\_SI\_001.PDF.
- [11] D. Braga, I. Gutiérrez Lezama, H. Berger, and A. F. Morpurgo, "Quantitative determination of the band gap of WS<sub>2</sub> with ambipolar ionic liquid-gated transistors," *Nano Lett*, vol. 12, no. 10, pp. 5218–5223, Oct. 2012, doi: 10.1021/NL302389D/SUPPL\_FILE/NL302389D\_SI\_001.PDF.
- [12] Q. He *et al.*, "Fabrication of Flexible MoS<sub>2</sub> Thin-Film Transistor Arrays for Practical Gas-Sensing Applications," *Small*, vol. 8, no. 19, pp. 2994–2999, Oct. 2012, doi: 10.1002/SMLL.201201224.
- [13] H. Jiang, L. Zheng, Z. Liu, and X. Wang, "Two-dimensional materials: From mechanical properties to flexible mechanical sensors," *InfoMat*, vol. 2, no. 6. 2020. doi: 10.1002/inf2.12072.

- [14] S. Imani Yengejeh, W. Wen, and Y. Wang, "Mechanical properties of lateral transition metal dichalcogenide heterostructures," *Front Phys (Beijing)*, vol. 16, no. 1, p. 13502, Feb. 2021, doi: 10.1007/s11467-020-1001-5.
- [15] T. Cui *et al.*, "Mechanical reliability of monolayer MoS<sub>2</sub> and WSe<sub>2</sub>," *Matter*, vol. 5, no. 9, pp. 2975–2989, Sep. 2022, doi: 10.1016/j.matt.2022.06.014.
- [16] K. Liu and J. Wu, "Mechanical properties of two-dimensional materials and heterostructures," *J Mater Res*, vol. 31, no. 7, 2016, doi: 10.1557/jmr.2015.324.
- [17] S. Bertolazzi, J. Brivio, and A. Kis, "Stretching and breaking of ultrathin MoS<sub>2</sub>," *ACS Nano*, vol. 5, no. 12, 2011, doi: 10.1021/nn203879f.
- [18] M. A. Islam *et al.*, "Fatigue Behavior of Polymer Encapsulated Graphene to Mitigate Interfacial Fatigue Damage," *Adv Eng Mater*, Sep. 2023, doi: 10.1002/adem.202300336.
- [19] R. Rizvi *et al.*, "High-Throughput Continuous Production of Shear-Exfoliated 2D Layered Materials using Compressible Flows," *Advanced Materials*, vol. 30, no. 30, Jul. 2018, doi: 10.1002/adma.201800200.
- [20] G. Eda, T. Fujita, H. Yamaguchi, D. Voiry, M. Chen, and M. Chhowalla, "Coherent atomic and electronic heterostructures of single-layer MoS<sub>2</sub>," *ACS Nano*, vol. 6, no. 8, pp. 7311–7317, Aug. 2012, doi: 10.1021/NN302422X/ASSET/IMAGES/MEDIUM/NN-2012-02422X\_0002.GIF.
- [21] A. N. Enyashin *et al.*, "New route for stabilization of 1T-WS<sub>2</sub> and MoS<sub>2</sub> phases," *Journal of Physical Chemistry C*, vol. 115, no. 50, pp. 24586–24591, Dec. 2011, doi: 10.1021/JP2076325/ASSET/IMAGES/MEDIUM/JP-2011-076325\_0006.GIF.
- [22] J. A. Wilson and A. D. Yoffe, "The transition metal dichalcogenides discussion and interpretation of the observed optical, electrical and structural properties," *Adv Phys*, 1969, doi: 10.1080/00018736900101307.
- [23] D. Voiry *et al.*, "Enhanced catalytic activity in strained chemically exfoliated WS<sub>2</sub> nanosheets for hydrogen evolution," *Nat Mater*, vol. 12, no. 9, pp. 850–855, 2013, doi: 10.1038/NMAT3700.
- [24] D. Voiry *et al.*, "Conducting MoS<sub>2</sub> nanosheets as catalysts for hydrogen evolution reaction," *Nano Lett*, vol. 13, no. 12, pp. 6222–6227, Dec. 2013, doi: 10.1021/NL403661S/SUPPL\_FILE/NL403661S\_SI\_001.PDF.
- [25] M. A. Lukowski, A. S. Daniel, F. Meng, A. Forticaux, L. Li, and S. Jin, "Enhanced hydrogen evolution catalysis from chemically exfoliated metallic MoS<sub>2</sub> nanosheets," *J Am Chem Soc*, vol. 135, no. 28, pp. 10274–10277, Jul. 2013, doi: 10.1021/JA404523S/SUPPL\_FILE/JA404523S\_SI\_001.PDF.
- [26] K.-A. N. Duerloo, Y. Li, and E. J. Reed, "Structural phase transitions in two-dimensional Mo- and W-dichalcogenide monolayers," *Nat Commun*, vol. 5, no. 1, p. 4214, Sep. 2014, doi: 10.1038/ncomms5214.
- [27] S. Cho *et al.*, "Phase patterning for ohmic homojunction contact in MoTe<sub>2</sub>," *Science (1979)*, vol. 349, no. 6248, pp. 625–628, Aug. 2015, doi: 10.1126/SCIENCE.AAB3175/SUPPL\_FILE/CHO-SM.PDF.

- [28] C. Gong *et al.*, “Electronic and Optoelectronic Applications Based on 2D Novel Anisotropic Transition Metal Dichalcogenides,” *Advanced Science*, vol. 4, no. 12, Dec. 2017, doi: 10.1002/ADVS.201700231.
- [29] Y. Q. Bie *et al.*, “A MoTe<sub>2</sub>-based light-emitting diode and photodetector for silicon photonic integrated circuits,” *Nature Nanotechnology* 2017 12:12, vol. 12, no. 12, pp. 1124–1129, Oct. 2017, doi: 10.1038/nnano.2017.209.
- [30] B. Yu *et al.*, “Outstanding Catalytic Effects of 1T'-MoTe<sub>2</sub> Quantum Dots@3D Graphene in Shuttle-Free Li-S Batteries,” *ACS Nano*, vol. 15, no. 8, pp. 13279–13288, Aug. 2021, doi: 10.1021/ACS.NANO.1C03011/SUPPL\_FILE/NN1C03011\_SI\_001.PDF.
- [31] S. Kang *et al.*, “Tunable Out-of-Plane Piezoelectricity in Thin-Layered MoTe<sub>2</sub> by Surface Corrugation-Mediated Flexoelectricity,” *ACS Appl Mater Interfaces*, vol. 10, no. 32, pp. 27424–27431, Aug. 2018, doi: 10.1021/ACSAMI.8B06325/SUPPL\_FILE/AM8B06325\_SI\_001.PDF.
- [32] C. Ruppert, O. B. Aslan, and T. F. Heinz, “Optical properties and band gap of single- and few-layer MoTe<sub>2</sub> crystals,” *Nano Lett*, vol. 14, no. 11, pp. 6231–6236, Nov. 2014, doi: 10.1021/NL502557G/SUPPL\_FILE/NL502557G\_SI\_001.PDF.
- [33] A. Conan, A. Bonnet, M. Zoeter, and D. Ramoul, “Dependence of the Total Mobility in a One-Band Model Application to n-Type MoTe<sub>2</sub>,” *physica status solidi (b)*, vol. 124, no. 1, pp. 403–410, Jul. 1984, doi: 10.1002/pssb.2221240144.
- [34] Y.-F. Lin *et al.*, “Ambipolar MoTe<sub>2</sub> Transistors and Their Applications in Logic Circuits,” *Advanced Materials*, vol. 26, no. 20, pp. 3263–3269, May 2014, doi: 10.1002/adma.201305845.
- [35] D. Jiang *et al.*, “Flexible electronics based on 2D transition metal dichalcogenides,” *J Mater Chem A Mater*, vol. 10, no. 1, pp. 89–121, 2022, doi: 10.1039/D1TA06741A.
- [36] L. Gao, “Flexible Device Applications of 2D Semiconductors,” *Small*, vol. 13, no. 35, p. 1603994, Sep. 2017, doi: 10.1002/sml.201603994.
- [37] Y. Tan *et al.*, “Controllable 2H-to-1T' phase transition in few-layer MoTe<sub>2</sub>,” *Nanoscale*, vol. 10, no. 42, pp. 19964–19971, Nov. 2018, doi: 10.1039/C8NR06115G.
- [38] S. A. Chowdhury *et al.*, “Mechanical Properties and Strain Transfer Behavior of Molybdenum Ditelluride (MoTe<sub>2</sub>) Thin Films,” *J Eng Mater Technol*, vol. 144, no. 1, pp. 1–10, 2022, doi: 10.1115/1.4051306.
- [39] H. Cheong, Y. Cheon, S. Y. Lim, and K. Kim, “Structural phase transition and interlayer coupling in few-layer 1T' and 2H MoTe<sub>2</sub>,” *ACS Nano*, vol. 15, no. 2, pp. 2962–2970, Feb. 2021, doi: 10.1021/ACS.NANO.0C09162/SUPPL\_FILE/NN0C09162\_SI\_001.PDF.
- [40] D. Vikraman *et al.*, “Fullerene-free, MoTe<sub>2</sub> atomic layer blended bulk heterojunctions for improved organic solar cell and photodetector performance,” *Journal of Materials Research and Technology*, vol. 17, pp. 2875–2887, Mar. 2022, doi: 10.1016/J.JMRT.2022.02.050.

- [41] S. Song, D. H. Keum, S. Cho, D. Perello, Y. Kim, and Y. H. Lee, "Room Temperature Semiconductor-Metal Transition of MoTe<sub>2</sub> Thin Films Engineered by Strain," *Nano Lett*, vol. 16, no. 1, 2016, doi: 10.1021/acs.nanolett.5b03481.
- [42] G. Mirabelli *et al.*, "Air sensitivity of MoS<sub>2</sub>, MoSe<sub>2</sub>, MoTe<sub>2</sub>, HfS<sub>2</sub>, and HfSe<sub>2</sub>," *J Appl Phys*, vol. 120, no. 12, p. 125102, Sep. 2016, doi: 10.1063/1.4963290.
- [43] Y. Sun *et al.*, "Elastic Properties and Fracture Behaviors of Biaxially Deformed, Polymorphic MoTe<sub>2</sub>," *Nano Lett*, vol. 19, no. 2, pp. 761–769, 2019, doi: 10.1021/acs.nanolett.8b03833.
- [44] B. Mortazavi, G. R. Berdiyrov, M. Makaremi, and T. Rabczuk, "Mechanical responses of two-dimensional MoTe<sub>2</sub>; pristine 2H, 1T and 1T' and 1T'/2H heterostructure," *Extreme Mech Lett*, vol. 20, pp. 65–72, Apr. 2018, doi: 10.1016/J.EML.2018.01.005.
- [45] R. V. Goldstein and N. F. Morozov, "Mechanics of deformation and fracture of nanomaterials and nanotechnology," *Physical Mesomechanics*, vol. 10, no. 5–6, pp. 235–246, 2007, doi: 10.1016/j.physme.2007.11.002.
- [46] A. N. Guz and Y. Y. Rushchitskii, "Nanomaterials: On the mechanics of nanomaterials," *International Applied Mechanics*, vol. 39, no. 11, pp. 1271–1293, Nov. 2003, doi: 10.1023/B:INAM.0000015598.53063.26/METRICS.
- [47] L. Guo, T. Kitamura, Y. Yan, T. Sumigawa, and K. Huang, "Fracture mechanics investigation on crack propagation in the nano-multilayered materials," *Int J Solids Struct*, vol. 64–65, pp. 208–220, Jul. 2015, doi: 10.1016/J.IJSOLSTR.2015.03.025.
- [48] B. Ni *et al.*, "Fracture at the two-dimensional limit," *MRS Bulletin*, vol. 47, no. 8. 2022. doi: 10.1557/s43577-022-00385-4.
- [49] M. Q. Le, "Fracture and strength of single-atom-thick hexagonal materials," *Comput Mater Sci*, vol. 201, p. 110854, Jan. 2022, doi: 10.1016/J.COMMATSCI.2021.110854.
- [50] J.-W. Jiang and Y.-P. Zhou, "Parameterization of Stillinger-Weber Potential for Two-Dimensional Atomic Crystals," in *Handbook of Stillinger-Weber Potential Parameters for Two-Dimensional Atomic Crystals*, vol. i, no. tourism, InTech, 2017, p. 13. doi: 10.5772/intechopen.71929.
- [51] M. A. Torkaman-Asadi and M. A. Kouchakzadeh, "Atomistic simulations of mechanical properties and fracture of graphene: A review," *Comput Mater Sci*, vol. 210, p. 111457, Jul. 2022, doi: 10.1016/J.COMMATSCI.2022.111457.
- [52] M. L. Pereira Júnior *et al.*, "On the Elastic Properties and Fracture Patterns of MoX<sub>2</sub> (X = S, Se, Te) Membranes: A Reactive Molecular Dynamics Study," *Condens Matter*, vol. 5, no. 4, p. 73, Nov. 2020, doi: 10.3390/condmat5040073.
- [53] D. Puotinen, R. E. Newnham, and IUCr, "The crystal structure of MoTe<sub>2</sub>," *urn:issn:0365-110X*, vol. 14, no. 6, pp. 691–692, Jun. 1961, doi: 10.1107/S0365110X61002084.
- [54] A. P. Thompson *et al.*, "LAMMPS - a flexible simulation tool for particle-based materials modeling at the atomic, meso, and continuum scales," *Comput Phys Commun*, vol. 271, p. 108171, Feb. 2022, doi: 10.1016/j.cpc.2021.108171.

- [55] J.-W. Jiang, "Parametrization of Stillinger–Weber potential based on valence force field model: application to single-layer MoS<sub>2</sub> and black phosphorus," *Nanotechnology*, vol. 26, no. 31, p. 315706, Jul. 2015, doi: 10.1088/0957-4484/26/31/315706.
- [56] V. T. Pham and T. H. Fang, "Effects of temperature and intrinsic structural defects on mechanical properties and thermal conductivities of InSe monolayers," *Scientific Reports 2020 10:1*, vol. 10, no. 1, pp. 1–15, Sep. 2020, doi: 10.1038/s41598-020-72162-9.
- [57] A. Mobaraki, A. Kandemir, H. Yapicioglu, O. Gülseren, and C. Sevik, "Validation of inter-atomic potential for WS<sub>2</sub> and WSe<sub>2</sub> crystals through assessment of thermal transport properties," *Comput Mater Sci*, vol. 144, pp. 92–98, Mar. 2018, doi: 10.1016/J.COMMATSCI.2017.12.005.
- [58] Z. D. Sha, Q. X. Pei, K. Zhou, Z. Dong, and Y. W. Zhang, "Temperature and strain-rate dependent mechanical properties of single-layer borophene," *Extreme Mech Lett*, vol. 19, pp. 39–45, Mar. 2018, doi: 10.1016/J.EML.2017.12.008.
- [59] J.-W. Jiang, "Misfit Strain-Induced Buckling for Transition-Metal Dichalcogenide Lateral Heterostructures: A Molecular Dynamics Study," *Acta Mechanica Solida Sinica*, vol. 32, no. 1, pp. 17–28, Feb. 2019, doi: 10.1007/s10338-018-0049-z.
- [60] K. Momma and F. Izumi, "VESTA: a three-dimensional visualization system for electronic and structural analysis," *J Appl Crystallogr*, vol. 41, no. 3, pp. 653–658, Jun. 2008, doi: 10.1107/S0021889808012016.
- [61] T. Ma *et al.*, "Growth of bilayer MoTe<sub>2</sub> single crystals with strong non-linear Hall effect," *Nat Commun*, vol. 13, no. 1, 2022, doi: 10.1038/s41467-022-33201-3.
- [62] Z. Yang, Y. Huang, F. Ma, Y. Sun, K. Xu, and P. K. Chu, "Temperature and strain-rate effects on the deformation behaviors of nano-crystalline graphene sheets," *European Physical Journal B*, vol. 88, no. 5, 2015, doi: 10.1140/epjb/e2015-50850-x.
- [63] W. Ding, D. Han, J. Zhang, and X. Wang, "Mechanical responses of WSe<sub>2</sub> monolayers: a molecular dynamics study," *Mater Res Express*, vol. 6, no. 8, p. 085071, May 2019, doi: 10.1088/2053-1591/AB2085.
- [64] M. M. Islam *et al.*, "ReaxFF molecular dynamics simulations on lithiated sulfur cathode materials," *Physical Chemistry Chemical Physics*, vol. 17, no. 5, pp. 3383–3393, 2015, doi: 10.1039/C4CP04532G.
- [65] R. A. S. I. Subad, T. S. Akash, P. Bose, and M. M. Islam, "Engineered defects to modulate fracture strength of single layer MoS<sub>2</sub>: An atomistic study," *Physica B Condens Matter*, vol. 592, no. October 2019, p. 412219, Sep. 2020, doi: 10.1016/j.physb.2020.412219.
- [66] T. Li, "Ideal strength and phonon instability in single-layer MoS<sub>2</sub>," *Phys Rev B Condens Matter Mater Phys*, vol. 85, no. 23, p. 235407, Jun. 2012, doi: 10.1103/PHYSREVB.85.235407/FIGURES/5/MEDIUM.
- [67] A. Stukowski, "Visualization and analysis of atomistic simulation data with OVITO—the Open Visualization Tool," *Model Simul Mat Sci Eng*, vol. 18, no. 1, p. 015012, Jan. 2010, doi: 10.1088/0965-0393/18/1/015012.

- [68] G. Wang *et al.*, "Recent advances in the mechanics of 2D materials," *International Journal of Extreme Manufacturing*, vol. 5, no. 3. 2023. doi: 10.1088/2631-7990/acdda2.
- [69] C. Yi, C. Hu, M. Bai, J. Lv, and D. Tang, "Molecular dynamics study on the mechanical properties of multilayer MoS<sub>2</sub> under different potentials," *Nanotechnology*, vol. 31, no. 21, 2020, doi: 10.1088/1361-6528/ab73b3.
- [70] S. A. Kazemi *et al.*, "Vacancy impacts on electronic and mechanical properties of MX<sub>2</sub> (M = Mo, W and X = S, Se) monolayers," *RSC Adv*, vol. 13, no. 10, 2023, doi: 10.1039/d3ra00205e.
- [71] J. W. Jiang and H. S. Park, "Mechanical properties of MoS<sub>2</sub>/graphene heterostructures," *Appl Phys Lett*, vol. 105, no. 3, p. 033108, Jul. 2014, doi: 10.1063/1.4891342.
- [72] V. T. Pham and T. H. Fang, "Thermal and mechanical characterization of nanoporous two-dimensional MoS<sub>2</sub> membranes," *Sci Rep*, vol. 12, no. 1, 2022, doi: 10.1038/s41598-022-11883-5.
- [73] Y. Han, P. Chen, J. Zhu, H. Liu, and Y. Zhang, "Mechanical behavior of single layer MoS<sub>2</sub> sheets with aligned defects under uniaxial tension," *J Appl Phys*, vol. 130, no. 12, 2021, doi: 10.1063/5.0061556.
- [74] K. Liu *et al.*, "Elastic properties of chemical-vapor-deposited monolayer MoS<sub>2</sub>, WS<sub>2</sub>, and their bilayer heterostructures," *Nano Lett*, vol. 14, no. 9, pp. 5097–5103, Sep. 2014, doi: 10.1021/NL501793A/SUPPL\_FILE/NL501793A\_SI\_001.PDF.
- [75] A. B. Alencar, A. B. de Oliveira, and H. Chacham, "Crystal reorientation and plastic deformation of single-layer MoS<sub>2</sub> and MoSe<sub>2</sub> under uniaxial stress," *Journal of Physics Condensed Matter*, vol. 33, no. 12, 2021, doi: 10.1088/1361-648X/abd5f5.
- [76] H. Tang, D. Hu, Z. Cui, H. Ye, and G. Zhang, "Effects of Defect and Temperature on the Mechanical Performance of WS<sub>2</sub>: A Multiscale Analysis," *Journal of Physical Chemistry C*, vol. 125, no. 4, 2021, doi: 10.1021/acs.jpcc.0c09897.
- [77] T. M. T. Oishi, P. Malakar, M. Islam, and M. M. Islam, "Atomic-scale perspective of mechanical properties and fracture mechanisms of graphene/WS<sub>2</sub>/graphene heterostructure," *Computational Condensed Matter*, vol. 29, 2021, doi: 10.1016/j.cocom.2021.e00612.
- [78] E. H. Chowdhury, M. H. Rahman, S. Fatema, and M. M. Islam, "Investigation of the mechanical properties and fracture mechanisms of graphene/WSe<sub>2</sub> vertical heterostructure: A molecular dynamics study," *Comput Mater Sci*, vol. 188, no. August 2020, p. 110231, Feb. 2021, doi: 10.1016/j.commatsci.2020.110231.
- [79] R. Zhang, V. Koutsos, and R. Cheung, "Elastic properties of suspended multilayer WSe<sub>2</sub>," *Appl Phys Lett*, vol. 108, no. 4, 2016, doi: 10.1063/1.4940982.
- [80] Y. Yang *et al.*, "Brittle Fracture of 2D MoSe<sub>2</sub>," *Advanced Materials*, vol. 29, no. 2, 2017, doi: 10.1002/adma.201604201.